scientific reports

Check for updates

OPEN

Sd-021, derivatives of decursin, inhibits tumorigenesis in NSCLC by inhibiting the EGFR/STAT3 signaling pathway

Hyun-Ha Hwang[1], Jeong-Hui Je[1], Hyeong-Chan Lee[1], Ji-Sung Yoo[1], Taehyoun Kim[1], Jung Hwan Choi[2], Jin Won Hong[2], Hae-In Lim[1], Ga Yoon Kim[1], Yun-Beom Sim[3,4], Kwang-Jin Cho[1,3,4], Eun-wook Choi[3,4], Chunhoo Cheon[1,4], Jae Yeol Lee[2]✉ & Seong-Gyu Ko[1,3,4]✉

Lung cancer, particularly non-small cell lung cancer (NSCLC), remains a significant challenge in oncology despite advances in targeted and immune-based therapies. NSCLC accounts for approximately 85% of all lung cancer cases, with five-year survival rates ranging from 4 to 17%, depending on disease stage and regional factors. Chemotherapy resistance remains a major hurdle, contributing to poor patient prognosis. This study explores the therapeutic potential of Sd-021, a novel decursinol derivative, compared to its parent compound, decursin, within various NSCLC cell lines. Our results reveal that Sd-021 demonstrates enhanced anticancer activity, highlighted by a more significant reduction in cell viability, increased induction of apoptosis, and more pronounced cell cycle arrest. Notably, Sd-021 shows increased inhibition of the EGFR/STAT3 signaling pathway in EGFR wild-type cell lines, including A549, H460, and H1299 cells. Moreover, in vivo experiments employing a subcutaneous xenograft mouse model reveal that Sd-021 reduces tumor volume with minimal systemic toxicity, as indicated by histopathological assessments revealing reduced tumor proliferation and heightened apoptosis. The minimal toxicity of Sd-021 offers reassurance regarding its safety for potential clinical applications. In conclusion, these findings highlight the promise of Sd-021 as a therapeutic agent against NSCLC.

Keywords Sd-021, Decursin derivatives, Non-small cell lung cancer (NSCLC), EGFR/STAT3 signaling pathway

Lung cancer continues to be a major global health issue and stands as the leading cause of cancer-related deaths[1,2]. Non-small cell lung cancer (NSCLC) represents about 85% of all lung cancer cases[3]. Despite progress in targeted therapies, including small-molecule tyrosine kinase inhibitors, and advances in immunotherapy, the prognosis for NSCLC patients remains generally poor[4]. This primarily results from the development of resistance to chemotherapy[4]. The five-year survival rates for NSCLC patients vary from 4 to 17%, depending on the disease stage and regional differences[5,6]. There is an urgent need to continue research into new therapeutic agents to enhance outcomes for NSCLC patients[4,5,7]. Historically, natural products have significantly contributed to cancer prevention and treatment, providing a rich source of bioactive compounds[8].

Epidermal Growth Factor Receptor (EGFR) is a tyrosine kinase receptor that regulates epithelial cell proliferation[9–11]. This transmembrane receptor is activated by binding extracellular ligands[9–11]. It interacts with other membrane receptors, particularly those in the erbB/HER family[12,13]. EGFR is significantly hyperactivated in various cancers, making it a vital therapeutic target in several solid tumors[14]. However, the effectiveness of EGFR tyrosine kinase inhibitors (TKIs) in patients with wild-type EGFR tumors is still debated[15–18]. In addition to emerging immune-based therapies, targeted treatments are highly effective in tumors driven by oncogenic

[1]Department of Science in Korean Medicine, Graduate School, Kyung Hee University, Seoul 02447, Republic of Korea. [2]Research Institute for Basic Sciences and Department of Chemistry, College of Sciences, Kyung Hee University, Seoul 02447, Republic of Korea. [3]Institute for Research Center in Jaein R&P, Seoul, Republic of Korea. [4]Korean Medicine-Based Drug Repositioning Cancer Research Center, College of Korean Medicine, Kyung Hee University, Seoul 02447, Republic of Korea. ✉email: ljy@khu.ac.kr; epiko@khu.ac.kr

mutations, though they benefit only a small fraction of cases[7,19]. Despite extensive research, searching for new therapeutic strategies for lung cancer remains ongoing.

Previous research described the synthesis of several decursinol derivatives, including Sd-021 (initially designated as MRC-D-004)[20]. This compound, synthesized through EDC-mediated coupling of an acryloyl group with an alcohol moiety, demonstrated notable anticancer activity in NSCLC cell lines[20]. The decursin, the parent compound of Sd-021, is well-documented as a promising natural-based anticancer agent effective against a range of malignancies, including melanoma, gastric, prostate, colon, breast, lung, glioblastoma, pancreatic, and ovarian cancers[21–28]. Sd-021, according to molecular docking analysis, acts as a JAK1 inhibitor through interactions with Leu959, Kis885, and Arg1007, thus confirming a structure-activity relationship that includes stereochemistry[20].

Although Sd-021 has demonstrated enhanced anticancer efficacy compared to decursin in the A549 cell line, the results are confined to this specific cell line, limiting our ability to conclusively prove its anticancer effectiveness across NSCLC. To address this issue, we plan to validate the anticancer efficacy of Sd-021 across various NSCLC cell lines and through in vivo experiments.

Results

The cytotoxicity of Sd-021 is enhanced compared to decursin in NSCLC cell lines

To evaluate the cytotoxic effects of Sd-021 in non-small cell lung cancer (NSCLC) cell lines, we conducted MTT assays after exposing cells to concentrations of 3.125, 6.25, 12.5, 25, and 50 μM for 24, 48, and 72 h. To evaluate the cytotoxic effects of decursin and Sd-021, MTT assays were performed on A549, H460, H1299, and HCC827 cell lines at 24, 48, and 72 h post-treatment. At 24 h, both compounds exhibited concentration-dependent cytotoxicity, particularly at 25 μM and 50 μM. Notably, Sd-021 induced a significantly greater reduction in cell viability than decursin across all tested cell lines at these concentrations. At 48 h, decursin showed significant cytotoxicity at 50 μM, while Sd-021 exhibited marked cytotoxic effects at 6.25, 12.5, 25, and 50 μM. At both 25 μM and 50 μM, Sd-021 treatment resulted in significantly lower cell viability compared to decursin treatment. By 72 h, Sd-021 consistently decreased cell viability at 6.25, 12.5, 25, and 50 μM in all four cell lines, with the extent of reduction being significantly greater than that of decursin at 12.5, 25, and 50 μM. These data collectively indicate that Sd-021 exerts a stronger cytotoxic effect than decursin in A549, H460, H1299, and HCC827 cells, in a dose- and time-dependent manner (Fig. 1A) (statistical analysis for this is provided in Supplementary Material 2). Moreover, clonogenic assays conducted over seven days, using concentrations ranging from 0.625 to 10 μM, demonstrated that Sd-021 inhibited colony count and formation more effectively than decursin, suggesting more significant cytotoxicity (Fig. 1B). These results confirm that decursin and its derivative, Sd-021, exert cytotoxic effects in NSCLC cell lines, with Sd-021 showing substantially more significant cytotoxicity than decursin.

Sd-021 is more effective at inducing cell cycle arrest and cell death than decursin

To assess the impact of Sd-021 on cell death, which showed enhanced suppression of viability compared to decursin, A549 cells were stained with 7-AAD and Annexin V and analyzed using flow cytometry. Following decursin treatment, an increase in the population in quadrant 2 was observed in all cell lines except HCC827. The percentage of cells in quadrant 2 was higher in the decursin-treated group compared to the Sd-021-treated group. In all cell lines, the percentage of cells in quadrants 1 and 4 increased compared to the control group, with a greater increase observed in the Sd-021-treated group than in the decursin-treated group. Additionally, the number of live cells in quadrant 3 decreased in both treatment groups compared to the control, with a more pronounced reduction in the Sd-021-treated group than in the decursin-treated group. Collectively, these findings indicate that Sd-021 induced greater cell death than decursin in all NSCLC cell lines tested. Furthermore, the significant increase in the populations in quadrants 1 and 4 in the Sd-021-treated group compared to the decursin-treated group suggests that Sd-021 more effectively induces apoptotic cell death. Therefore, Sd-021 appears to be more potent than decursin in promoting apoptotic cell death in NSCLC cell lines (Fig. 2A). To further investigate the involvement of apoptotic pathways in Sd-021-induced cell death, we examined the expression levels of apoptosis-related proteins by western blot analysis. To investigate the apoptotic mechanisms underlying Sd-021-induced cytotoxicity, we examined the expression of cleaved caspase-3, cleaved caspase-8, and cleaved PARP by western blot analysis across all NSCLC cell lines. Cleaved caspase-3 expression was detected in all Sd-021-treated cell lines; however, densitometric analysis revealed no statistically significant differences compared to the control or decursin-treated groups. In contrast, cleaved caspase-8 was also observed in all Sd-021-treated cell lines. Quantitative analysis demonstrated a significant increase in cleaved caspase-8 expression in A549 cells at 12.5, 25, and 50 μM, and in H1299 cells at 50 μM. Notably, in both A549 and H1299 cells, 50 μM Sd-021 treatment resulted in markedly higher cleaved caspase-8 levels compared to decursin. Although cleaved caspase-8 signals were detectable in HCC827 and H460 cells following Sd-021 treatment, these did not reach statistical significance upon quantification. Nevertheless, cleaved PARP levels were elevated in both HCC827 and H460 cells upon Sd-021 treatment, and were consistently higher than those observed with decursin, suggesting that Sd-021 may induce apoptosis more effectively via PARP cleavage in these cell lines (Fig. 2B). Taken together, these results suggest that Sd-021 induces apoptotic cell death more effectively than decursin in NSCLC cell lines, highlighting its potential as a more potent apoptotic inducer in this context. To determine the extent to which these compounds effectively induce cell cycle arrest, A549 cells were analyzed by PI staining to determine cell cycle distribution. In A549 and H1299 cells, an increase in the G1/G0 phase and a decrease in the S and G2/M phases were observed; however, there was no significant difference between decursin and Sd-021 treatments. In contrast, in HCC827 and H460 cells, a decrease in the G2/M phase was observed, along with the induction of sub-G1/G0 phase arrest. Notably, in H460 cells, Sd-021 treatment resulted in a statistically significant difference compared to decursin, whereas in HCC827 cells, the changes in the sub-G1/G0 and G2/M phases showed a trend but were not statistically significant (Fig. 3A). To further investigate the molecular mechanisms associated

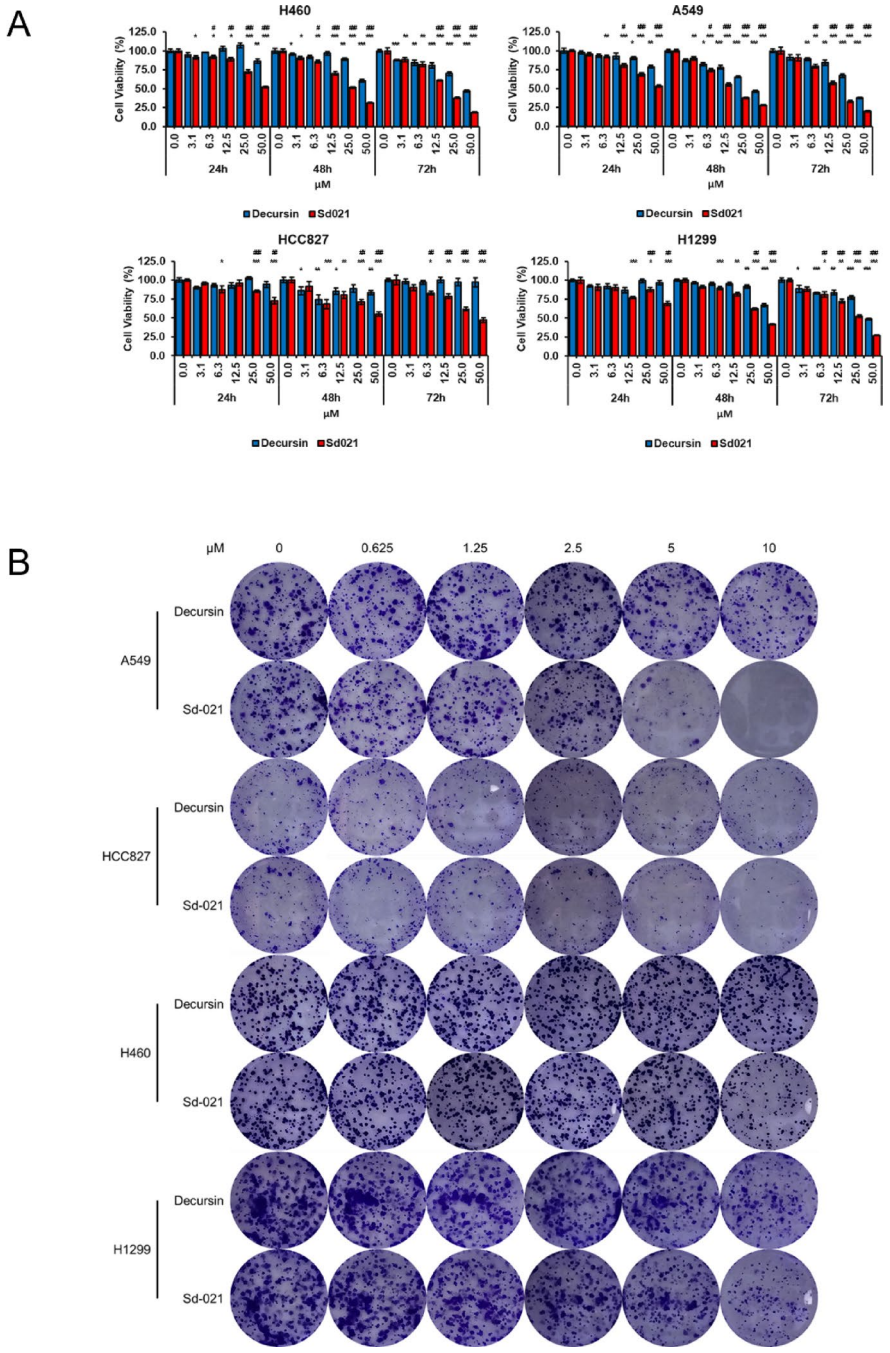

Fig. 1. Comparison of the effects of decursin and Sd-021 on inhibiting viability in NSCLC cell lines. (**A**) Results from the MTT assay after treating A549, H460, H1299, and HCC827 cells with decursin or Sd-021 in a concentration-dependent manner (3.125, 6.25, 12.5, 25, and 50 μM) and time-dependent manner (24, 48, and 72 h). The data are expressed as mean ± standard deviation. Statistical analysis was performed using unpaired *t*-tests. *Indicates comparison with 0 μM; # indicates comparison with decursin at the same concentration. Significance levels: $p < 0.05$ (* or #), $p < 0.01$ (** or ##), $p < 0.001$ (*** or ###). (**B**) Outcomes from the clonogenic assay displaying colony formation after treatment of A549, H460, H1299, and HCC827 cells with decursin or Sd-021 at varying concentrations (0.625, 1.25, 2.5, 5, and 10 μM).

with cell cycle regulation, we examined the expression levels of phosphorylated retinoblastoma protein (p-Rb) following treatment with Sd-021 and decursin in NSCLC cell lines. As shown in Fig. 3B, p-Rb expression was consistently suppressed at 50 μM Sd-021 in all tested cell lines, indicating a robust inhibitory effect on Rb phosphorylation. Taken together, these findings suggest that both Sd-021 and decursin induce G1/S phase cell cycle arrest and apoptosis in NSCLC cells, at least in part through the suppression of p-Rb.

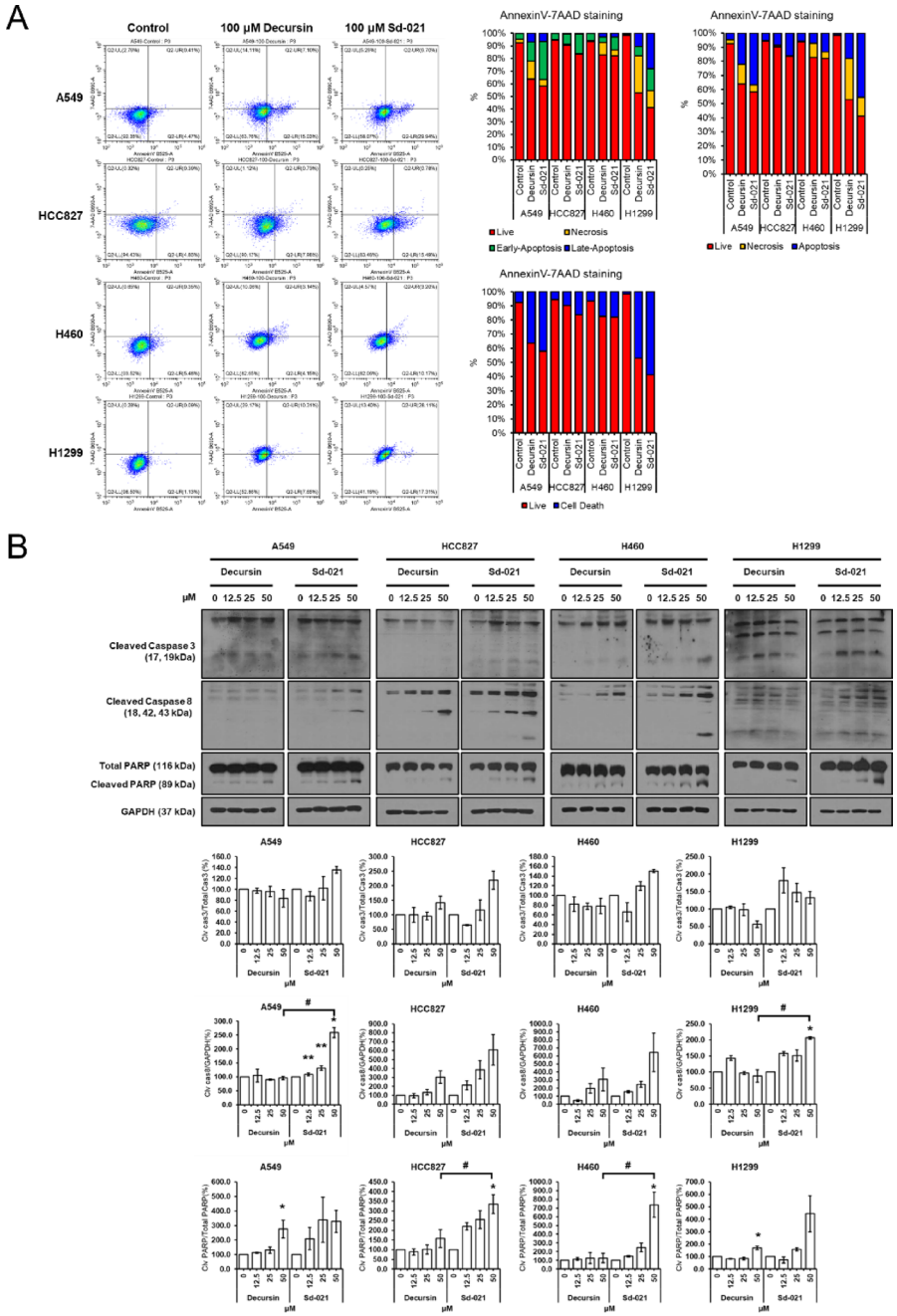

Fig. 2. Comparison of the effects of decursin and Sd-021 on inducing cell death in NSCLC cell lines. (**A**) Results of the cell death marker analysis via western blot after treating A549, H460, H1299, and HCC827 cells with decursin or Sd-021 in a concentration-dependent manner (12.5, 25, and 50 μM) Original blots are presented in (Fig. S1A–D). (**B**) Outcomes of Annexin V & 7AAD staining obtained from flow cytometry after treating A549, H460, and H1299 cells with decursin or Sd-021 at 25 and 50 μM concentrations. Quantified band intensities were normalized to GAPDH. Cleaved PARP levels were normalized to total PARP. Statistical analysis was performed using two-way ANOVA with Tukey's post-hoc test. : vs. 0 μM; #: vs. Decursin. Significance: $p < 0.05$ (* or #), < 0.01 (** or ##), < 0.001 (*** or ###).

Sd-021 inhibits the EGFR/STAT3 pathway in EGFR wild-type lung cancer cell lines

Following observations that Sd-021 reduces cell viability in NSCLC cell lines, we postulated that it might also suppress cell proliferation. To assess the effect of Sd-021 on EGFR signaling, we examined the p-EGFR(Y1068) following treatment with Sd-021 and decursin. In both A549 and H460 cells, 50 μM Sd-021 significantly reduced p-EGFR(Y1068) expression levels, whereas decursin failed to inhibit EGFR phosphorylation in these cell lines. Moreover, the inhibition of p-EGFR(Y1068) by Sd-021 was significantly greater than that observed with decursin at the same concentration. In contrast, although a reduction in p-EGFR(Y1068) signal was observed

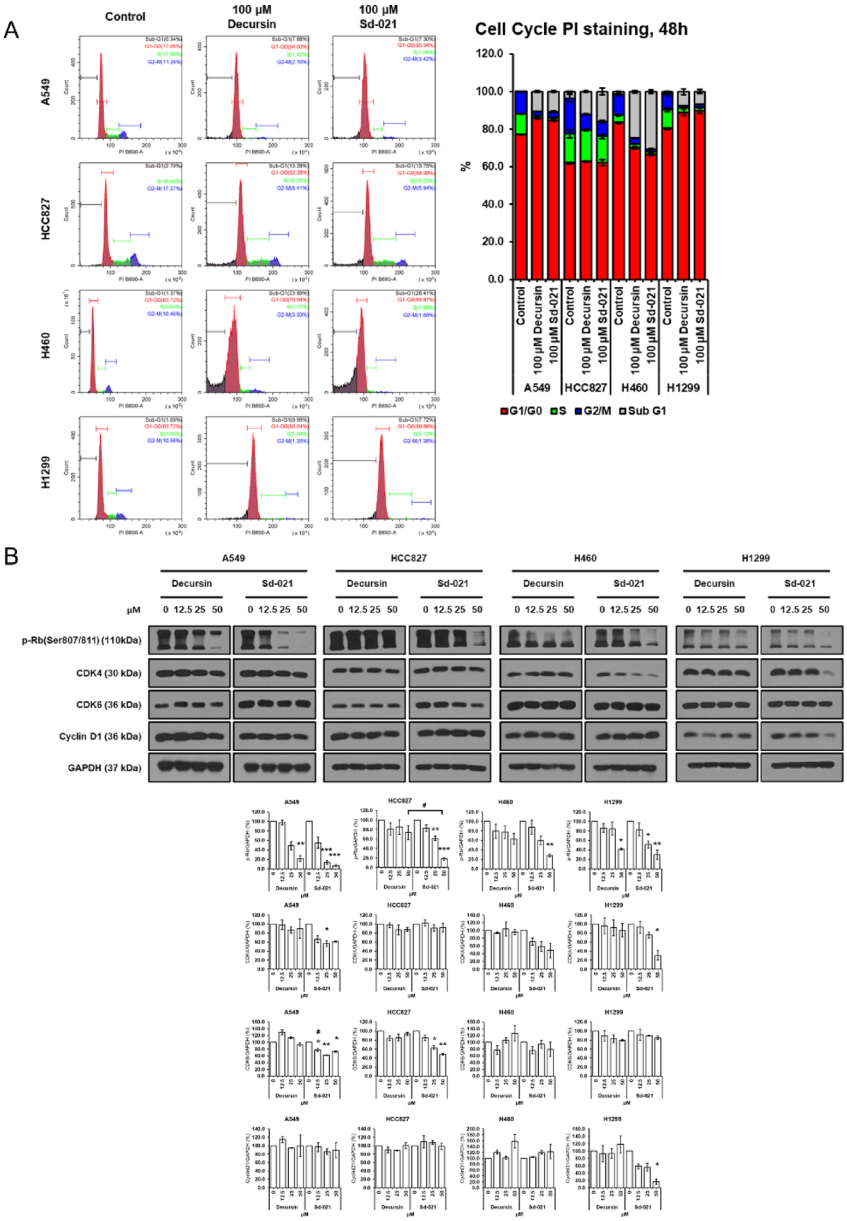

Fig. 3. Comparison of the effects of decursin and Sd-021 on cell cycle arrest in NSCLC cell lines. (**A**) Results of PI staining from flow cytometry following treatment of A549, H460, and H1299 cells with decursin or Sd-021 at 25, 50 and 100 μM concentrations. (**B**) Results of cell cycle marker analysis conducted through western blot after treating A549, H460, H1299, and HCC827 cells with decursin or Sd-021 in a concentration-dependent manner (12.5, 25, and 50 μM). Original blots are presented in (Fig. S2A–E). Quantified band intensities were normalized to GAPDH. Statistical analysis was performed using two-way ANOVA with Tukey's post-hoc test. : vs. 0 μM; #: vs. Decursin. Significance: $p < 0.05$ (* or #), < 0.01 (** or ##), < 0.001 (*** or ###).

in HCC827 and H1299 cells treated with 50 μM Sd-021, the changes were not statistically significant based on densitometric analysis. Notably, in the EGFR mutant type HCC827, p-EGFR(Y1068) was not inhibited, whereas inhibition of phosphorylation was evident in EGFR wild-type (EGFR wt) cell lines[29–31]. Moreover, to determine whether Sd-021 modulates downstream signaling of EGFR, we assessed the p-STAT3, a key effector in the EGFR signaling cascade. Across all NSCLC cell lines tested, treatment with 50 μM Sd-021 led to a significant reduction in p-STAT3 protein levels compared to the untreated control. Notably, in HCC827 cells, Sd-021 induced a more pronounced decrease in p-STAT3 levels than decursin at the same concentration, indicating a stronger inhibitory effect on the STAT3 pathway (Fig. 4). These results indicate that Sd-021 effectively suppresses the activation of STAT3 in NSCLC cell lines.

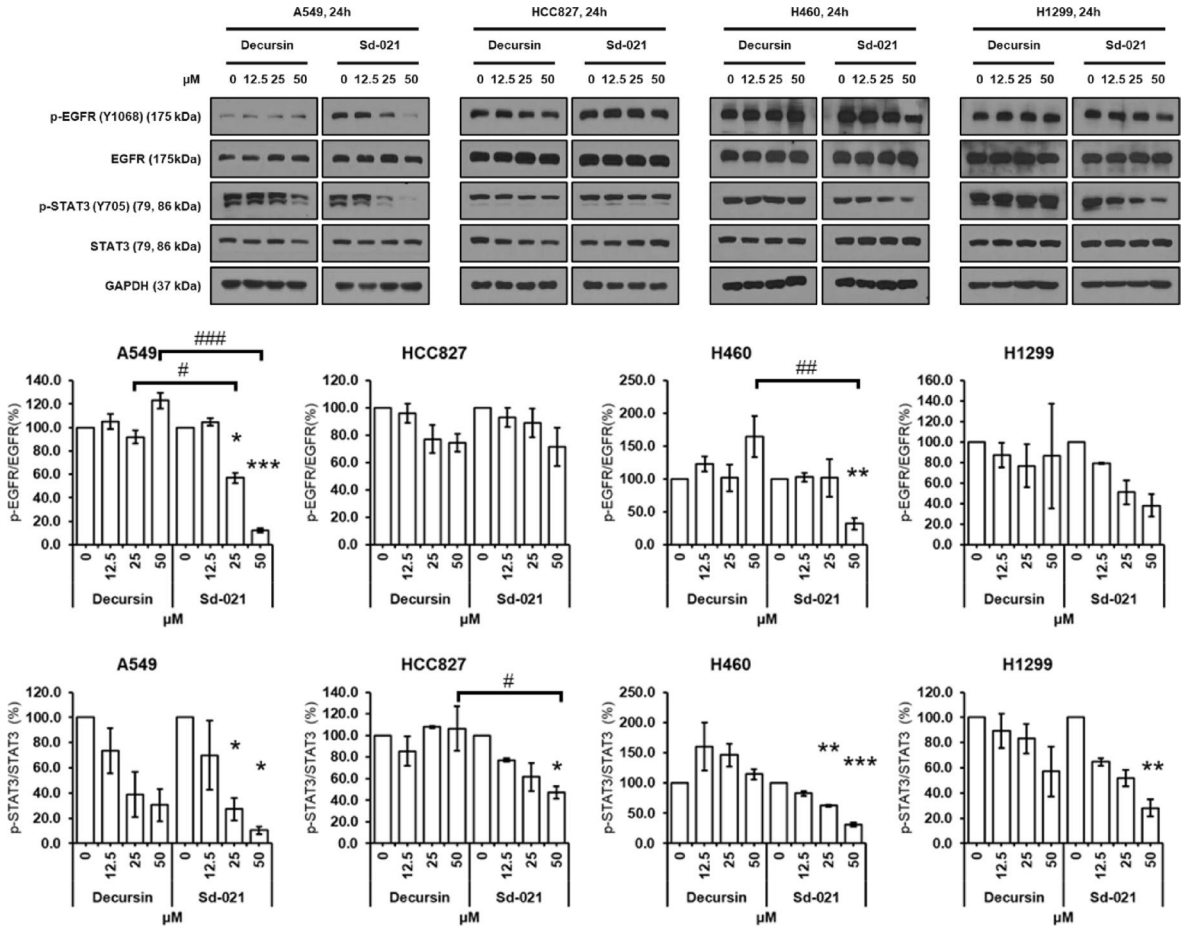

Fig. 4. The EGFR/STAT3 pathway was analyzed using western blot after treating A549, H460, H1299, and HCC827 cells with decursin or Sd-021 in a concentration-dependent manner at 12.5, 25, and 50 μM. Raw data of western band are presented in (Fig. S3A–E). Phospho-EGFR (p-EGFR) levels were normalized to total EGFR, and phospho-STAT3 (p-STAT3) levels were normalized to total STAT3. Statistical analysis was performed using two-way ANOVA with Tukey's post-hoc test. vs. 0 μM; #: vs. Decursin. Significance: $p < 0.05$ (* or #), < 0.01 (** or ##), < 0.001 (*** or ###).

Sd-021 inhibits tumorigenesis in the subcutaneous xenograft mouse model

In our study, we aimed to evaluate the potential of Sd-021 to inhibit tumor formation in vivo using a subcutaneous xenograft mouse model. To evaluate the anti-tumorigenic effects of Sd-021 and decursin, we administered vehicle, 30 mg/kg decursin, 3 mg/kg Sd-021, and 30 mg/kg Sd-021 to tumor-bearing mice and assessed tumor growth inhibition (Fig. 5A–C). The xenograft study was conducted over a period of 27 days from the first day of drug administration, with treatments given three times per week. At the experimental endpoint, tumor size was significantly reduced in the group treated with 30 mg/kg Sd-021. In contrast, no statistically significant reduction in tumor growth was observed in the 30 mg/kg decursin or 3 mg/kg Sd-021 treatment groups. Furthermore, the 30 mg/kg Sd-021 group exhibited significantly smaller tumor size compared to the 3 mg/kg Sd-021 group. However, the tumor size reduction in the 30 mg/kg Sd-021 group was not statistically significant compared to the 30 mg/kg decursin group. Nonetheless, both the 30 mg/kg Sd-021 and 30 mg/kg decursin treatment groups showed smaller tumor volumes compared to the vehicle control group, suggesting a potential dose-dependent anti-tumor effect (Fig. 5C) Moreover, there was no significant difference in body weight changes between the control and the 30 mg/kg decursin-treated groups throughout the experimental period, indicating no apparent systemic toxicity. In addition, a CYP inhibition assay was conducted to assess potential drug–enzyme interactions. Sd-021 did not exhibit inhibitory activity against CYP1A2, CYP2C19, CYP2D6, or CYP3A4, suggesting a low likelihood of cytochrome P450-mediated drug interactions (Table 1). indicating an absence of systemic toxicity at this dosage. After sacrifice, tumor tissues were collected and analyzed. Histological analysis using hematoxylin and eosin (H&E) staining revealed a marked reduction in tumor cell density in the 30 mg/kg Sd-021-treated group compared to the vehicle group (Fig. 5D). In contrast, the tumor tissues from mice treated with decursin did not show a significant difference in cancer cell density relative to the control. Immunohistochemical staining further demonstrated increased cleaved caspase-3 and cleaved PARP-positive cells in the 30 mg/kg Sd-021-treated tumors, indicating enhanced apoptosis. Notably, cleaved caspase-3 expression was significantly higher in the Sd-021-treated group than in the decursin-treated group. Although cleaved PARP intensity also appeared

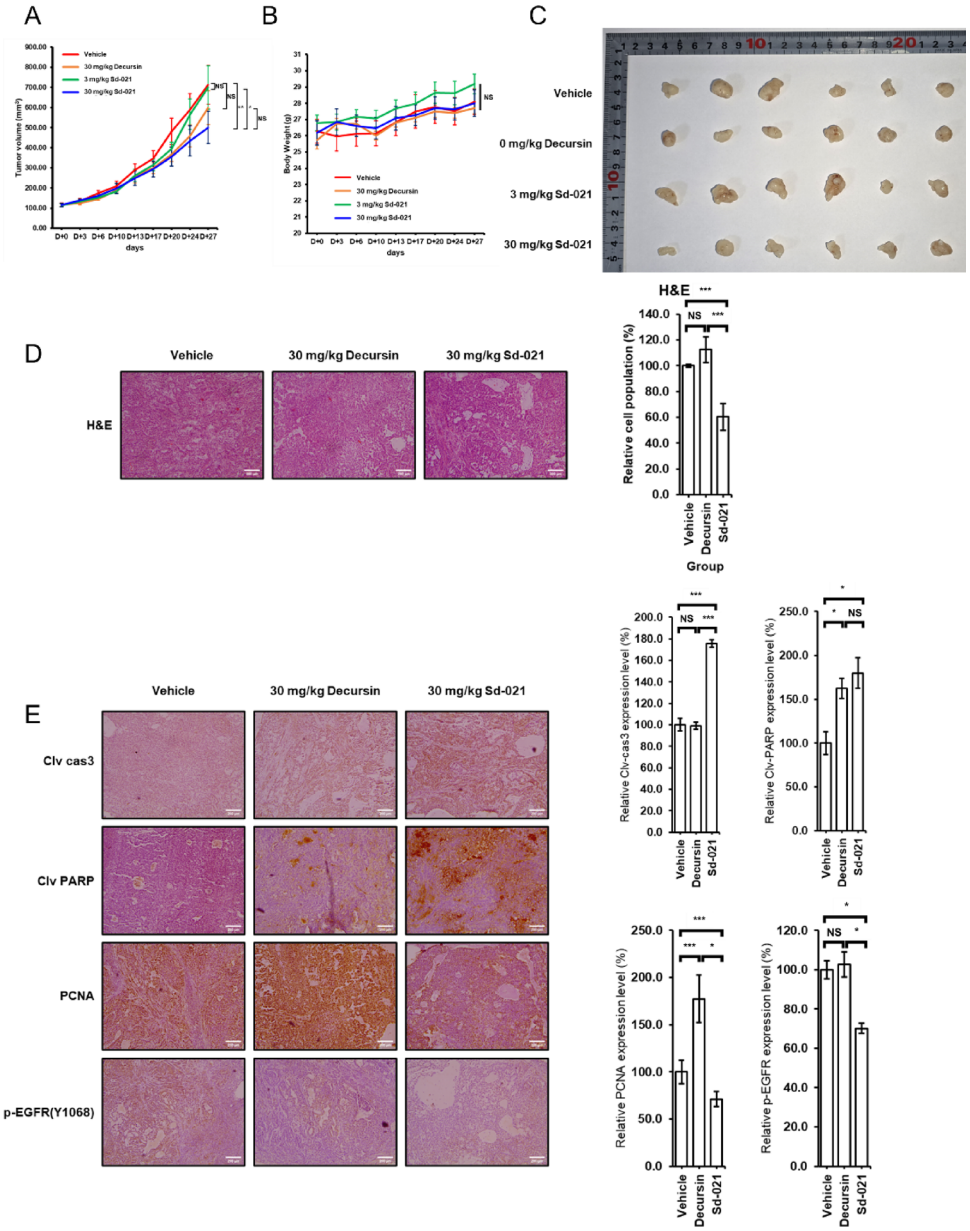

Fig. 5. Comparison of the efficacy of decursin and Sd-021 in a subcutaneous xenograft model using A549 mice. (**A**) Tumor growth curves were plotted to monitor changes in body weight and tumor volume post-implantation, and tumor xenografts were subsequently excised for analysis. (**B**) Body weight was tracked to assess the general health condition. (**C**) Image of excised tumor tissues from each treatment group. (**D**) hematoxylin and eosin (HE) staining images of tumor sections from different treatment groups, illustrating tissue morphology and cellular structure. (**E**) Immunohistochemical staining of tumor sections from each group, showing positive staining indicated by brown coloration. Images were taken using an eyepiece magnification of 0.63x and an objective lens magnification of 40x. The scale bar represents 20 µm. Data are expressed as mean ± SD, with $n = 6$. The statistical comparison among the three groups was performed using one-way ANOVA, followed by Tukey's post-hoc test for multiple comparisons. Statistical significance was indicated using p-values or symbolic annotations ($^{*}p < 0.05$, $^{**}p < 0.01$, $^{***}p < 0.001$, *ns* not significant) in the corresponding figure.

stronger in the Sd-021 group, this difference did not reach statistical significance when compared to decursin treatment (Fig. 5E). Immunohistochemical staining demonstrated decreased PCNA expression, suggesting reduced cell proliferation (Fig. 5E). The group treated with Sd-021 exhibited greater inhibition compared to both the vehicle and decursin groups (Fig. 5E). Immunohistochemical analysis of tumor tissues revealed that p-EGFR-positive cells were not significantly reduced in the decursin-treated group compared to the vehicle group. In contrast, the Sd-021-treated group showed a marked suppression of p-EGFR expression. Quantification confirmed that p-EGFR levels were significantly lower in the Sd-021-treated group than in the decursin-treated

	Filename	Area ratio mean (area/ISTD area) ± SD	%R
Acetaminophen(1A2)	Control	0.394 ± 0.023	100
	Ketoconazole(reference)	0.41 ± 0.012	104.2
	0.1 µM Sd-021	0.417 ± 0.008	106
	0.5 µM Sd-021	0.415 ± 0.019	105.5
	2 µM Sd-021	0.405 ± 0.006	102.9
	10 µM Sd-021	0.371 ± 0.005	94.1
4'-hydroxydiclofenac(2C9)	Control	2.74 ± 0.113	100
	Ketoconazole(reference)	2.911 ± 0.074	106.2
	0.1 µM Sd-021	2.974 ± 0.012	108.5
	0.5 µM Sd-021	2.892 ± 0.106	105.5
	2 µM Sd-021	2.713 ± 0.004	99
	10 µM Sd-021	1.858 ± 0.023	67.8
4'-hydroxymephenytoin(2C19)	Control	0.051 ± 0.001	100
	Ketoconazole(reference)	0.056 ± 0.003	111.1
	0.1 µM Sd-021	0.056 ± 0.003	109.8
	0.5 µM Sd-021	0.054 ± 0	107
	2 µM Sd-021	0.054 ± 0.001	106.2
	10 µM Sd-021	0.045 ± 0.002	88.6
Dextrophan(2D6)	Control	0.676 ± 0.068	100
	Ketoconazole(reference)	0.748 ± 0.032	110.6
	0.1 µM Sd-021	0.601 ± 0.004	89
	0.5 µM Sd-021	0.696 ± 0.074	102.9
	2 µM Sd-021	0.746 ± 0.009	110.3
	10 µM Sd-021	0.62 ± 0.01	91.7
1'-hydroxymidazolam(3A4)	Control	1.506 ± 0.089	100
	Ketoconazole(reference)	0.405 ± 0.007	26.9
	0.1 µM Sd-021	1.613 ± 0.036	107.1
	0.5 µM Sd-021	1.633 ± 0.041	108.4
	2 µM Sd-021	1.672 ± 0.023	111
	10 µM Sd-021	1.414 ± 0.014	93.9

Table 1. CYP inhibition assay of Sd-021. IC_{50} values (µM) for each derivative against the CYP enzyme were calculated from percent activity values measured after a 15 min incubation at each concentration using Phoenix WinNonlin software. Area/ Internal Standard(ISTD) area represents the peak area of the analyte normalized to the peak area of the ISTD. Ketoconazole (0.1 µM) was used as a positive control, with its % control activity (acceptance range: 25% ± 10%) serving as an internal evaluation criterion. SD represents the standard deviation of duplicate measurements. %R represents the relative activity (%) of each sample based on the mean Area Ratio compared to the control. Inhibitory potency was classified based on IC_{50} as potent (<1 µM), moderate (1–10 µM), or no/weak (>10 µM).

group, indicating a stronger inhibitory effect on EGFR activation. These results support our findings and further validate the potential of Sd-021 as a promising anticancer agent in NSCLC treatment strategies.

Discussion

The results of this study offer valuable insights into the anticancer properties of Sd-021, especially regarding non-small cell lung cancer (NSCLC). Building upon earlier studies that established decursin as a powerful natural anticancer agent[9,32,33] we found that Sd-021, a derivative of decursin, exhibits improved anticancer activities. This is evident from its capability to suppress tumor growth and activate apoptotic pathways both in vivo and in vitro.

Our in vitro assays indicate that Sd-021 exerts a more pronounced cytotoxic effect than decursin in several NSCLC cell lines, including A549, H460, H1299, and HCC827[29]. Notably, the compound was particularly effective in reducing cell viability and colony formation, suggesting its strong inhibitory effects on cell proliferation and survival. These effects are likely mediated through the modulation of critical regulatory proteins involved in the cell cycle and apoptosis, including p-Rb (Ser807/811), cyclin D1, CDK4, cleaved caspase 3 and cleaved caspase 8[33,34]. Previous studies have suggested that CDK4/6 inhibitors induce G1/G0 phase arrest and reduce p-Rb levels[35,36]. In line with these findings, our study demonstrated that Sd-021 also effectively induced G1/G0 phase arrest. While CDK4 and CDK6 levels were not significantly reduced, the observed decrease in p-Rb suggests that

Treatment with Sd-021 led to a consistent reduction in p-Rb levels across all NSCLC cell lines, suggesting that Sd-021 may induce apoptosis through G1/S phase cell cycle arrest.

Interestingly, although both Sd-021 and decursin inhibited the phosphorylation of STAT3 in EGFR wild-type cell lines[37–39]our results underscore a differential response based on EGFR mutation status[30]suggesting that genetic alterations may influence the therapeutic efficacy of these compounds. This observation indicates the need for further investigation to understand the molecular mechanisms underlying the variable responses to treatment, especially across genetically distinct NSCLC subtypes[4,29,30,40]. Although Sd-021 treatment led to a consistent reduction in p-STAT3 levels across NSCLC cell lines, this pattern of inhibition did not fully correlate with that of p-EGFR suppression. While STAT3 is widely recognized as a downstream effector of EGFR signaling, it is also known to be regulated by multiple upstream pathways due to the complex nature of intracellular signaling cascades. Therefore, the observed suppression of STAT3 phosphorylation by Sd-021 may not be solely dependent on EGFR inhibition. Despite its ability to inhibit p-STAT3, the precise upstream targets of Sd-021 responsible for this effect remain unidentified. Further studies are warranted to elucidate the direct molecular targets of Sd-021 and to define its specific mechanism of action in NSCLC.In our xenograft model, although the tumor volume reduction in the Sd-021 treatment group was not statistically significant, the average tumor sizes were consistently smaller compared to the control and decursin groups. Our results demonstrate that Sd-021 significantly reduced tumor volume compared to the vehicle group; however, statistical analysis revealed that this reduction was not significantly different from that observed in the decursin-treated group. Histological analysis confirmed reduced PCNA expression and increased cleaved caspase-3 positive cells, highlighting the effectiveness of Sd-021 in promoting apoptosis. Although Sd-021 did not significantly inhibit tumor volume growth in this in vivo study, IHC staining suggests that prolonged administration may lead to tumor volume suppression. Furthermore, the absence of significant changes in body weight during the study indicates the potential for higher dosage administration. The CYP inhibition assay revealed that Sd-021 exhibits low inhibitory activity against major cytochrome P450 isoforms, including CYP1A2, CYP2C19, CYP2D6, and CYP3A4, suggesting it is a compound with minimal risk of CYP-mediated drug interactions. However, slight inhibition of CYP1A2 activity was observed, indicating a potential safety concern in patients with bleeding risk, as CYP1A2 is involved in the metabolism of certain anticoagulants. Importantly, the lack of CYP3A4 inhibition suggests that Sd-021 may be suitable for combination therapies with a wide range of anticancer agents, offering potential for synergistic therapeutic effects. Therefore, Sd-021 holds promise as a potential anticancer agent for NSCLC through long-term treatment.

The consistent results across various experimental platforms emphasize the potential of Sd-021 as a promising candidate for further development as a therapeutic agent against NSCLC. Moreover, considering the complexity of cancer pathogenesis, particularly the dynamic nature of tumor evolution and drug resistance, exploring combination therapy strategies involving Sd-021 could potentially enhance therapeutic outcomes by targeting multiple pathways and overcoming resistance mechanisms.

Conclusion

Based on the collective findings of this study, Sd-021 demonstrates strong potential as a novel anticancer agent for non-small cell lung cancer (NSCLC), supported by its ability to induce G1/S phase arrest, inhibit p-Rb and p-STAT3 signaling, and promote apoptosis both in vitro and in vivo. Although the reduction in tumor volume was not statistically significant, histopathological evidence of decreased proliferation and increased apoptosis suggests therapeutic efficacy upon prolonged administration. Importantly, Sd-021 exhibits minimal CYP inhibition, particularly sparing CYP3A4, highlighting its suitability for combination therapy with reduced risk of drug–drug interactions. The selective inhibition of CYP1A2, while noteworthy, indicates the need for cautious consideration in specific clinical scenarios. Overall, these findings position Sd-021 as a promising candidate for further development in NSCLC treatment, potentially as part of a combination strategy to overcome resistance and improve therapeutic outcomes.

Methods

Cell culture

The A549 human lung adenocarcinoma cell line was sourced from the American Type Culture Collection (ATCC) and maintained in Dulbecco's Modified Eagle Medium (DMEM, LM001-05, WELGENE) supplemented with 10% fetal bovine serum (FBS, 16000-044, GIBCO) and 1% antibiotic-antimycotic solution (LS203-01, WELGENE). These cells were incubated at 37 °C in a humidified atmosphere containing 5% CO_2. Other human lung carcinoma cell lines, such as H460, H1299, and HCC827, were acquired from the Korean Cell Line Bank (KCLB) and maintained in RPMI1640 (LS001-01, WELGENE) with 10% fetal bovine serum and 1% antibiotic-antimycotic solution. These cells were incubated at 37 °C in an atmosphere with 5% CO_2. Culture media were replaced every two to three days, and once cell confluence reached 80–90%, they were subcultured using a trypsin-EDTA solution.

MTT assay

For the MTT assay, A549 cells were seeded in 96-well plates at a density of 2,500 cells per well and exposed to various concentrations of DMSO (used as a control), Decursin or its derivatives were treated for 24, 48 and 72 h hours at final concentrations of 0, 3.125, 6.25, 12.5, 25, and 50 µM. Subsequently, MTT reagent (3-(4,5-Dimethylthiazol-2-yl)-2,5-diphenyltetrazolium bromide, D8418, Sigma Aldrich) was added to each well to facilitate formazan crystal formation. The cells were then incubated with MTT reagent for 2 h at 37 °C in a humidified environment containing 5% CO_2. Post-incubation, the MTT solution was carefully removed, DMSO added to dissolve the formazan crystals and lyse the cells, and cell viability was assessed by measuring the optical

density (OD) at 570 nm. The IC_{50} values for cell viability were calculated using the AAT Bioquest web-based tools(https://www.aatbio.com/tools/ic50-calculator) .

Colony formation assay

For the colony formation assay, A549 cells were seeded in 6-well plates at a density of 1,000 cells per well. The cells underwent treatment with DMSO (as the control), Decursin or Sd-021 were treated at concentrations of 0, 1.25, 2.5, 5, and 10 μM and the treatment period lasted 7 days to allow sufficient colony formation. Following treatment, the resulting colonies were stained and counted using the method Franken et al. (2006) described in the publication "Clonogenic assay of cells ."[32].

Western blot assay

The cells were seeded at a density of 150,000 cells per well and treated with DMSO (as control), Decursin, or Sd-021 for 24 h. Cell lysis was accomplished using RIPA buffer supplemented with PMSF, DTT, NaF, Na_3VO_4, and a protease inhibitor cocktail. The lysates were maintained on ice for 30 min, then centrifuged at 13,000 rpm for 30 min at 4 °C. The supernatant was subsequently collected for protein quantification. Protein concentrations were measured using the Bradford assay to ensure uniform loading for subsequent SDS-PAGE. The proteins were combined with sample buffer, separated by SDS-PAGE, and transferred to a PVDF membrane pre-soaked in methanol. The membrane was blocked with 5% skim milk and incubated overnight at 4 °C with primary antibodies: PARP (9542, 1:1000, CST), Cleaved Caspase 3 (9661, 1:1000, CST), Cleaved Caspase 8 (9496, 1:1000, CST), p-Rb(Ser807/811) (8516, 1:1000, CST), CDK2 (2546, 1:1000, CST), Cyclin D1 (2978, 1:1000, CST), EGFR (2232, 1:1000, CST), p-EGFR(Y1068) (3777, 1:1000, CST), CDK4 (12790, 1:1000, CST), CDK6 (13331, 1:1000, CST) p-STAT3 (9145, 1:1000, CST), STAT3 (4904, 1:1000, CST), and GAPDH (5174, 1:1000, CST). The following day, the membrane was incubated for 1 h at room temperature with secondary antibodies: anti-mouse (5450-0011, 1:5000, Seracare) and anti-rabbit (5450-0010, 1:5000, Seracare). Protein bands were visualized using a chemiluminescent substrate (DG-WP250, WELGENE) in a dark room. Quantification of the proteins detected by Western blot was performed using ImageJ software.

Flow cytometry (Annexin V/7-AAD staining)

Annexin V/7-AAD double staining was used to detect cell death through flow cytometry. A549 cells were cultured in 60 mm^2 dishes and treated with 100 μM Decursin and Sd-021. Following 72 h of treatment, the cells were harvested by trypsinization and centrifuged at 1,500 rpm for 10 min to remove the supernatant. The cell pellet was washed with cold DPBS and centrifuged under similar conditions. The Annexin V binding solution was prepared according to the manufacturer's instructions (BMS500FI, Invitrogen) by mixing Annexin V with the binding buffer. The A549 cell pellet was resuspended in this solution and transferred to a round-bottom tube, where it was incubated in the dark at room temperature for 15 min. After this, 7-AAD was added to the Annexin V binding solution, and the cells were incubated for 15 min. Flow cytometric analysis was conducted using a CytoFLEX Flow Cytometer (Beckman Coulter, USA), with at least 10,000 cells analyzed per sample. Data were analyzed using CytExpert software.

Flow cytometry (PI staining)

DNA cell cycle analysis was conducted using propidium iodide (PI) staining. Cells were harvested, prepared as a single-cell suspension, and washed twice in PBS, followed by centrifugation at 300 × g for 5 min. The resulting pellet was resuspended at a concentration of $3–6 \times 10^6$ cells/mL, and 500 μL of this suspension was transferred to a 15 mL polypropylene tube. Ethanol fixation was performed by slowly adding 5 mL of 70% ethanol while gently vortexing to prevent cell clumping, and the cells were fixed in 70% ethanol at -20 °C for at least 1 h or stored for several weeks before staining. Fixed cells were then washed twice in PBS and centrifuged at 300 × g for 5 min after each wash. The cell pellet was resuspended in 1 mL of PI staining solution, which contained 3.8 mM sodium citrate, 50 μg/mL PI (P4170, Sigma) in PBS, and 50 μL of 10 μg/mL RNase A stock solution (Worthington Biochemicals, boiled for 5 min, aliquoted, and stored at -20 °C). Cells were mixed thoroughly and incubated overnight at 4 °C for DNA staining. Samples were stored at 4 °C until analysis. Flow cytometric analysis was conducted using a CytoFLEX Flow Cytometer (Beckman Coulter, USA), with at least 10,000 events recorded per sample. Data were analyzed using CytExpert software.

Xenograft

BALB/c-nude male mice (6–7 weeks old, purchased from JaBio) were used to establish the xenograft model. All animal handling and experimental procedures were approved by the Institutional Animal Care and Use Committee (IACUC) under protocol IACUC2401-015 and conducted in accordance with IACUC guidelines, the Animal Protection Act, and the Act on the Protection and Management of Laboratory Animals. All methods were carried out following relevant guidelines and regulations and are reported in accordance with ARRIVE guidelines (https://arriveguidelines.org)[41]. Mice were housed in individually ventilated cages (ASPEN, TAPVEI), maintaining an environment of 20–26 °C, 30–70% relative humidity, and a 12-hour light/dark cycle. Animals received standard pelleted feed (SAFE® 40, SAFE®, France) and water ad libitum. Cage bedding was regularly replaced, and all handling and husbandry procedures followed institutional regulations. Mice were anesthetized with 2–3% isoflurane, and A549 cells (5×10^6 cells in 50 μL of PBS mixed with 50 μL of Matrigel for a total volume of 100 μL) were injected subcutaneously into the flank region. The injection site was sterilized with 70% ethanol before injection. Each group consisted of six mice, and the drug was dissolved in a vehicle solution prepared with Tween 80: PEG400: Ethanol: 5% Glucose = 1:6:3:20. Drug administration was performed three times per week via oral gavage at doses of 30 mg/kg decursin, 3 mg/kg Sd-021, and 30 mg/kg Sd-021, with a total administration volume of 100 μL per dose, based on a 25 g mouse. Mice were monitored daily for tumor

development and general health. Tumor size was measured using digital calipers, and the volume was calculated using the formula:

$$Tumor\ Volume = \frac{Length \times Width^2}{2}$$

Tumor monitoring was conducted three times weekly. Following ethical guidelines, mice were euthanized when the tumor volume reached approximately 1,500 mm^3 or if signs of distress were observed. The gas was introduced at a flow rate equivalent to approximately 60% of 4.2 L per minute. Following this, cervical dislocation was performed, and the tumor was excised. All methods are reported in accordance with ARRIVE guidelines to ensure transparency and reproducibility in animal research[42].

Hematoxylin and eosin staining

Hematoxylin and eosin (HE) staining was conducted to assess tissue morphology. Tissue sections were deparaffinized in xylene for 5 min, repeated twice, followed by rehydration through a graded ethanol series (100, 95, 70%) for 3 min each and rinsed in distilled water for 3 min. Sections were stained with hematoxylin (Merck, cat. no. 1.09253) for 30 s, and subsequently rinsed in running tap water for 3 min to allow differentiation. Sections were then dipped in acid alcohol (0.3% HCl in 70% ethanol) for a few seconds, followed by rinsing in tap water for 1 min and washing in distilled water three times for 3 min each. Eosin staining (Merck, cat. no. 1.09844) was performed for 2 min, followed by dehydration through a graded ethanol series (70, 95, and 100%) for 3 min each. Sections were cleared in xylene for 5 min, repeated twice, and coverslips were mounted using a suitable mounting medium. Slides were allowed to dry at room temperature. HE histologic analysis was quantified using ImageJ software.

Immunohistochemistry staining

Immunohistochemistry (IHC) was performed to evaluate the expression of specific markers in tissue sections. On day 1, sections were deparaffinized in xylene for 3 min, repeated twice, followed by rehydration through a graded ethanol series (100%, 95%, and 70%) for 3 min each. Endogenous peroxidase activity was blocked by incubating sections with 3% hydrogen peroxide (H_2O_2) for 2 min. Antigen retrieval was conducted by incubating the sections in 0.01 M sodium citrate buffer (pH 6.0) at boiling temperature for 10 min, followed by cooling at room temperature for 20 min and washing with PBS containing 0.1% Triton X-100 for 3 min. This was followed by two washes with PBS for 3 min each. To further block endogenous peroxidases, sections were treated with 3.5% H_2O_2 in 10% methanol for 15 min, then washed three times with PBS for 3 min each. A PAP pen was used to draw a hydrophobic barrier around each section. Non-specific binding was blocked by incubating the sections with normal goat serum for 1 h at room temperature, followed by three washes with PBS for 3 min each. Primary antibodies, including PCNA (1:200, 05-347, Millipore), cleaved caspase-3 (1:200, 9661, CST), cleaved PARP (1:100, sc-56196, santacruz), and p-EGFR (Y1068) (1:100, 3777, CST), diluted in blocking buffer, were applied to the sections and incubated overnight at 4 °C. On Day 2, slides were washed in PBS containing 0.1% Tween 20 for 3 min, followed by two washes with PBS for 5 min each. Sections were incubated with biotinylated secondary antibody (10 µL) diluted in 30 µL blocking buffer and 2 mL PBS for 1 h at room temperature. Slides were washed in PBS containing 0.1% Tween 20 for 3 min, followed by two additional washes with PBS for 3 min each. ABC reagent was prepared by mixing reagent A (40 µL) and reagent B (40 µL) in 2 mL PBS, 30 min before use. Sections were incubated with the ABC reagent for 30 min at room temperature, followed by three washes with PBS for 3 min each. DAB staining was performed by applying a DAB substrate solution, followed by washing the sections in distilled water three times for 3 min each. Counterstaining was performed by dipping the sections twice in hematoxylin, followed by an immediate transfer to distilled water for 30 s and washing in distilled water three times for 3 min each. Slides were dehydrated through a graded ethanol series (70, 95, and 100%) for 3 min each, followed by two washes in xylene for 5 min each. Coverslips were mounted using a suitable mounting medium, and the slides were allowed to dry at room temperature. Histological analysis was quantified using ImageJ software.

CYP inhibition assay

Compound Sd-021 was evaluated for its inhibitory effects on five major cytochrome P450 (CYP) isozymes, CYP1A2, CYP2C9, CYP2C19, CYP2D6, and CYP3A4, using pooled human liver microsomes (Corning, Cat. #452117). The incubation mixture (final volume 200 µL) contained human liver microsomes at 0.25 mg/mL in 0.1 M potassium phosphate buffer (pH 7.4; Corning, Cat. #451201), a substrate cocktail including phenacetin (50 µM; Sigma-Aldrich, Cat. #77440), diclofenac (10 µM; Sigma-Aldrich, Cat. #D6899), S-mephenytoin (100 µM; Sigma-Aldrich, Cat. #UC175), dextromethorphan (5 µM; Sigma-Aldrich, Cat. #81091), and midazolam (2.5 µM; Korea FDA), and the test compound Sd-021 at concentrations of 0.1, 0.5, 2, and 10 µM. Following a 5-min preincubation at 37 °C, the reactions were initiated by addition of an NADPH-regenerating system (Promega, Cat. #V9510) and allowed to proceed for 15 min at 37 °C. The reactions were terminated with ice-cold acetonitrile containing the internal standard terfenadine (Sigma-Aldrich, Cat. #T9562), followed by centrifugation at 15,000 rpm for 5 min at 4 °C. The resulting supernatants were analyzed by LC–MS/MS using a Nexera XR UHPLC system (Shimadzu, Japan) coupled to a TSQ Vantage triple quadrupole mass spectrometer (Thermo Scientific, USA). Separation was performed on a Kinetex C18 column (2.1 × 100 mm, 2.6 µm; Phenomenex, USA) using a mobile phase composed of 0.1% formic acid in water (A) and 0.1% formic acid in acetonitrile (B) under gradient elution. Metabolites, acetaminophen (Sigma-Aldrich, Cat. #A7085), 4′-hydroxydiclofenac (TRC, Cat. #H825225), 4′-hydroxymephenytoin (Santa Cruz, Cat. #sc210197), dextrorphan (Sigma-Aldrich, Cat. #UC205), and 1′-hydroxymidazolam (Sigma-Aldrich, Cat. #UC430), were detected using multiple reaction

monitoring (MRM) mode in Xcalibur software (Thermo, version 4.4). Percent enzyme activity relative to no-inhibitor control was calculated, and IC_{50} values were determined using Phoenix WinNonlin software (v6.4; Certara, USA) based on the inhibitory effect model. The assay performance was validated with ketoconazole (0.1 µM; Sigma-Aldrich, Cat. #K1003), a selective CYP3A4 inhibitor, which yielded the expected inhibition of 1′-hydroxymidazolam formation (~25% of control activity).

Statistical analysis

All statistical analyses were conducted using Microsoft® Excel® LTSC for Windows (Version 16.0.14332.20777). Data from at least three independent experiments are presented as mean ± standard deviation (SD). Differences between the two groups were assessed using an unpaired Student's *t*-test. Statistical analysis of the Western blot data was performed using two-way ANOVA followed by Tukey's multiple comparisons test. The statistical comparison among the three groups was performed using one-way ANOVA, followed by Tukey's post-hoc test for multiple comparisons. Statistical significance is mentioned in the figure legends. A p-value < 0.05 was considered statistically significant.

Data availability

The datasets used and/or analyzed during the current study available from thecorresponding author on reasonable request.

Received: 1 November 2024; Accepted: 4 June 2025
Published online: 02 July 2025

References

1. Mathieu, L. N. et al. FDA approval summary: Capmatinib and Tepotinib for the treatment of metastatic NSCLC harboring MET exon 14 skipping mutations or alterations. *Clin. Cancer Res.* **28**, 249–254. https://doi.org/10.1158/1078-0432.CCR-21-1566 (2022).
2. Bray, F. et al. Global cancer statistics 2018: GLOBOCAN estimates of incidence and mortality worldwide for 36 cancers in 185 countries. *CA Cancer J. Clin.* **68**, 394–424. https://doi.org/10.3322/caac.21492 (2018).
3. Wang, J. & Wu, L. First-line immunotherapy for advanced non-small cell lung cancer: current progress and future prospects. *Cancer Biol. Med.* **21**, 117–124. https://doi.org/10.20892/j.issn.2095-3941.2023.0401 (2023).
4. Min, H. Y. & Lee, H. Y. Mechanisms of resistance to chemotherapy in non-small cell lung cancer. *Arch. Pharm. Res.* **44**, 146–164. https://doi.org/10.1007/s12272-021-01312-y (2021).
5. Fu, K., Xie, F., Wang, F. & Fu, L. Therapeutic strategies for EGFR-mutated non-small cell lung cancer patients with osimertinib resistance. *J. Hematol. Oncol.* **15**, 173. https://doi.org/10.1186/s13045-022-01391-4 (2022).
6. Lahiri, A. et al. Lung cancer immunotherapy: progress, pitfalls, and promises. *Mol. Cancer*. **22**, 40. https://doi.org/10.1186/s12943-023-01740-y (2023).
7. Li, Y. et al. Toward the next generation EGFR inhibitors: an overview of osimertinib resistance mediated by EGFR mutations in non-small cell lung cancer. *Cell. Commun. Signal.* **21**, 71. https://doi.org/10.1186/s12964-023-01082-8 (2023).
8. Zhang, Q. Y., Wang, F. X., Jia, K. K. & Kong, L. D. Natural product interventions for chemotherapy and Radiotherapy-Induced side effects. *Front. Pharmacol.* **9**, 1253. https://doi.org/10.3389/fphar.2018.01253 (2018).
9. Yarden, Y. The EGFR family and its ligands in human cancer. Signalling mechanisms and therapeutic opportunities. *Eur. J. Cancer*. **37** (Suppl 4), 3–8. https://doi.org/10.1016/s0959-8049(01)00230-1 (2001).
10. Lemmon, M. A. & Schlessinger, J. Cell signaling by receptor tyrosine kinases. *Cell* **141**, 1117–1134. https://doi.org/10.1016/j.cell.2010.06.011 (2010).
11. Zhang, X., Gureasko, J., Shen, K., Cole, P. A. & Kuriyan, J. An allosteric mechanism for activation of the kinase domain of epidermal growth factor receptor. *Cell* **125**, 1137–1149. https://doi.org/10.1016/j.cell.2006.05.013 (2006).
12. Ciardiello, F. & Tortora, G. EGFR antagonists in cancer treatment. *N Engl. J. Med.* **358**, 1160–1174. https://doi.org/10.1056/NEJMra0707704 (2008).
13. Uribe, M. L., Marrocco, I. & Yarden, Y. EGFR in cancer: signaling mechanisms, drugs, and acquired resistance. *Cancers (Basel)* https://doi.org/10.3390/cancers13112748 (2021).
14. Camp, E. R. et al. Molecular mechanisms of resistance to therapies targeting the epidermal growth factor receptor. *Clin. Cancer Res.* **11**, 397–405 (2005).
15. Cappuzzo, F. et al. Erlotinib as maintenance treatment in advanced non-small-cell lung cancer: a multicentre, randomised, placebo-controlled phase 3 study. *Lancet Oncol.* **11**, 521–529. https://doi.org/10.1016/S1470-2045(10)70112-1 (2010).
16. Gatzemeier, U. et al. Phase III study of erlotinib in combination with cisplatin and gemcitabine in advanced non-small-cell lung cancer: the Tarceva lung Cancer investigation trial. *J. Clin. Oncol.* **25**, 1545–1552. https://doi.org/10.1200/JCO.2005.05.1474 (2007).
17. Zhao, N., Zhang, X. C., Yan, H. H., Yang, J. J. & Wu, Y. L. Efficacy of epidermal growth factor receptor inhibitors versus chemotherapy as second-line treatment in advanced non-small-cell lung cancer with wild-type EGFR: a meta-analysis of randomized controlled clinical trials. *Lung Cancer*. **85**, 66–73. https://doi.org/10.1016/j.lungcan.2014.03.026 (2014).
18. Ranson, M. Epidermal growth factor receptor tyrosine kinase inhibitors. *Br. J. Cancer*. **90**, 2250–2255. https://doi.org/10.1038/sj.bjc.6601873 (2004).
19. Weng, M. S., Chang, J. H., Hung, W. Y., Yang, Y. C. & Chien, M. H. The interplay of reactive oxygen species and the epidermal growth factor receptor in tumor progression and drug resistance. *J. Exp. Clin. Cancer Res.* **37**, 61. https://doi.org/10.1186/s13046-018-0728-0 (2018).
20. Ahn, J. et al. Antiproliferative activity and molecular Docking analysis of both enantiomerically pure Decursin derivatives as anticancer agents. *Chem. Pharm. Bull.* **72**, 498–506 (2024). Synthesis.
21. Chang, S. N. et al. Decursinol Angelate arrest melanoma cell proliferation by initiating cell death and tumor shrinkage via induction of apoptosis. *Int. J. Mol. Sci.* **22** https://doi.org/10.3390/ijms22084096 (2021).
22. Kim, S. et al. Decursin inhibits tumor growth, migration, and invasion in gastric cancer by down-regulating CXCR7 expression. *Am. J. Cancer Res.* **9**, 2007– (2019).
23. Choi, S. R. et al. Decursin from Angelicagigas Nakai induces apoptosis in RC-58T/h/SA#4 primary human prostate cancer cells via a mitochondria-related caspase pathway. *Food Chem. Toxicol.* **49**, 2517–2523. https://doi.org/10.1016/j.fct.2011.06.016 (2011).
24. Kim, D., Go, S. H., Song, Y., Lee, D. K. & Park, J. R. Decursin induces G1 cell cycle arrest and apoptosis through reactive oxygen species-mediated endoplasmic reticulum stress in human colorectal cancer cells in in vitro and xenograft models. *Int. J. Mol. Sci.* **25** https://doi.org/10.3390/ijms25189939 (2024).
25. Jiang, C. et al. Decursin and decursinol Angelate inhibit estrogen-stimulated and estrogen-independent growth and survival of breast cancer cells. *Breast Cancer Res.* **9**, R77. https://doi.org/10.1186/bcr1790 (2007).

26. Jung, M. Y. et al. Analysis and identification of active compounds from Gami-Soyosan toxic to MCF-7 human breast adenocarcinoma cells. *Biomolecules* **9** https://doi.org/10.3390/biom9070272 (2019).
27. Kim, J. et al. Decursin enhances TRAIL-induced apoptosis through oxidative stress mediated- Endoplasmic reticulum stress signalling in non-small cell lung cancers. *Br. J. Pharmacol.* **173**, 1033–1044. https://doi.org/10.1111/bph.13408 (2016).
28. Choi, H. S. et al. Decursin in Angelica gigas Nakai (AGN) enhances doxorubicin chemosensitivity in NCI/ADR-RES ovarian Cancer cells via Inhibition of P-glycoprotein expression. *Phytother Res.* **30**, 2020–2026. https://doi.org/10.1002/ptr.5708 (2016).
29. Huang, H. et al. EGFR mutations induce the suppression of CD8(+) T cell and anti-PD-1 resistance via ERK1/2-p90RSK-TGF-beta axis in non-small cell lung cancer. *J. Transl Med.* **22**, 653. https://doi.org/10.1186/s12967-024-05456-5 (2024).
30. Wang, F. et al. Phosphorylated EGFR expression May predict outcome of EGFR-TKIs therapy for the advanced NSCLC patients with wild-type EGFR. *J. Exp. Clin. Cancer Res.* **31**, 65. https://doi.org/10.1186/1756-9966-31-65 (2012).
31. Cheng, C. C. et al. YM155 as an inhibitor of cancer stemness simultaneously inhibits autophosphorylation of epidermal growth factor receptor and G9a-mediated stemness in lung cancer cells. *PLoS One.* **12**, e0182149. https://doi.org/10.1371/journal.pone.0182149 (2017).
32. Franken, N. A., Rodermond, H. M., Stap, J., Haveman, J. & van Bree, C. Clonogenic assay of cells in vitro. *Nat. Protoc.* **1**, 2315–2319. https://doi.org/10.1038/nprot.2006.339 (2006).
33. Chu, Y. et al. A comprehensive review of the anticancer effects of Decursin. *Front. Pharmacol.* **15**, 1303412. https://doi.org/10.3389/fphar.2024.1303412 (2024).
34. Viktorsson, K. & Lewensohn, R. Apoptotic signaling pathways in lung cancer. *J. Thorac. Oncol.* **2**, 175–179. https://doi.org/10.1097/JTO.0b013e318031cd78 (2007).
35. Cai, Z. et al. Overexpressed Cyclin D1 and CDK4 proteins are responsible for the resistance to CDK4/6 inhibitor in breast cancer that can be reversed by PI3K/mTOR inhibitors. *Sci. China Life Sci.* **66**, 94–109. https://doi.org/10.1007/s11427-021-2140-8 (2023).
36. Karim, B. O., Rhee, K. J., Liu, G., Zheng, D. & Huso, D. L. Chemoprevention utility of Silibinin and Cdk4 pathway Inhibition in Apc(-/+) mice. *BMC Cancer.* **13**, 157. https://doi.org/10.1186/1471-2407-13-157 (2013).
37. Tolomeo, M. & Cascio, A. The multifaced role of STAT3 in Cancer and its implication for anticancer therapy. *Int. J. Mol. Sci.* **22** https://doi.org/10.3390/ijms22020603 (2021).
38. Ahn, K. S. Special issue role of STAT3 in oncogenesis. *Biomedicines* **10** https://doi.org/10.3390/biomedicines10112689 (2022).
39. Harada, D., Takigawa, N. & Kiura, K. The role of STAT3 in Non-Small cell lung Cancer. *Cancers (Basel).* **6**, 708–722. https://doi.org/10.3390/cancers6020708 (2014).
40. Zhang, T. et al. Discovery of a novel third-generation EGFR inhibitor and identification of a potential combination strategy to overcome resistance. *Mol. Cancer.* **19**, 90. https://doi.org/10.1186/s12943-020-01202-9 (2020).
41. Kilkenny, C., Browne, W. J., Cuthill, I. C., Emerson, M. & Altman, D. G. Improving bioscience research reporting: the ARRIVE guidelines for reporting animal research. *PLoS Biol.* **8**, e1000412. https://doi.org/10.1371/journal.pbio.1000412 (2010).
42. du Percie, N. et al. Reporting animal research: explanation and elaboration for the ARRIVE guidelines 2.0. *PLoS Biol.* **18**, e3000411. https://doi.org/10.1371/journal.pbio.3000411 (2020).

Acknowledgements

The authors thank various departments and research centers at Kyung Hee University for their support and contributions, including the Department of Science in Korean Medicine, Graduate School, the Research Institute for Basic Sciences, and the Department of Chemistry, College of Sciences, for their invaluable assistance. Additionally, our appreciation extends to the Institute for Research Center in Jaein R&P for providing resources and the Korean Medicine-Based Drug Repositioning Cancer Research Center, College of Korean Medicine, Kyung Hee University, for their essential collaboration in completing this research.

Author contributions

S.-G. Ko, J.-Y. Lee, and H.-H. Hwang were responsible for the conceptualization and design of the research. The primary experiments were carried out by H.-H. Hwang, J.-S. Yoo, J.-H. Je, H.-C. Lee, H.-I. Lim, and G.-Y. Kim. H.-H. Hwang, T. Kim, J.-S. Yoo, J.-H. Je, and H.-C. Lee contributed to the revision and additional data collection. Data organization was managed by H.-H. Hwang. Data analysis was collaboratively conducted by H.-H. Hwang, J.-H. Choi, J.-W. Hong, K.-J. Cho, and E.-W. Choi. The initial manuscript draft was prepared by H.-H. Hwang, Y.-B. Sim, S.-G. Ko, and J.-Y. Lee. S.-G. Ko and E.-W. Choi provided supervision throughout the study and critically reviewed the manuscript. All authors contributed to the experiments, participated in data collection, and approved the final version of the manuscript for publication.

Funding

The research was supported by the Ministry of Science and ICT (MSIT) (No. 2020R1A5A2019413). This work was supported by the Starting Growth Technological R&D Program (TIPS Program, No. 00273170), funded by the Ministry of SMEs and Startups (MSS, Korea) in 2023.

Declarations

Competing interests

The authors declare no competing interests.

Additional information

Supplementary Information The online version contains supplementary material available at https://doi.org/10.1038/s41598-025-05715-5.

Correspondence and requests for materials should be addressed to J.Y.L. or S.-G.K.